Pressure Distributions on the Bottom of a Planing Hull During Slamming

Carolyn Q. JUDGE [1],
United States Naval Academy, United States

Abstract. Bottom pressures were measured on two prismatic planing hull models operating in regular waves. Testing in regular waves created repeated wave slam events, which provided information on variability of the motions, accelerations, and pressures during wave slamming events. Using a reconstructed pressure distribution based on Rosen's method [2] and predicted pressure distributions based on empirical equations given by Morabito [3], better understanding of how the hull and water interact during wave slamming can be achieved.

Keywords. planing hull, wave impact, impact pressures, pressure distribution, regular waves, fluid-structure interaction

1. Introduction

High-speed planing boats are subject to repeated slamming impacts, which can cause structural damage and discomfort or injury to passengers. Currently, the primary planing hull structural guideline [1] relies heavily on semi-empirical criteria that can have limited application. These guidelines provide conservative estimates leading for structural design, but lack specific guidance for allowing strategic reduction in structural weight. Structural design depends on knowing the hull bottom pressures, yet information about the magnitudes of peak pressures, time durations, and distribution over the hull is generally not available. Model tests conducted at the US Naval Academy measured the bottom pressures on a prismatic planing hull geometry during operation in waves. Pressures were measured at point locations to examine how pressures evolve over a wave slam event.

Rosen [2] presents a method for reconstructing the momentary pressure distribution on the hull bottom during a hull-water impact based on point pressure measurements. This method allows the timed measured pressures of a propagating pressure segment in one position of the hull at one instant in time to be associated with other positions at other instants in time. Morabito [3] presents an empirical method for calculating the pressure distribution on the bottom of prismatic planing hulls operating in calm water. The method can be extended to the impact problem by use of an "equivalent" planing velocity. This paper compares the planing pressures predicted by Morabito's empirical method with the recreated pressure distribution determined from Rosen's method for a planing hull geometry operating in regular waves.

[1] Corresponding Author: Carolyn Q. Judge, United States Naval Academy; E-mail: judge@usna.edu.

2. Description of Model Experiment

The experiments used a prismatic planing hull model tested in the 115.8 meter (380 ft) long tow tank channel located at the United States Naval Academy. The model was free in heave and pitch and constrained in all other degrees of freedom. The model geometry is shown in Figure 1. Heave, pitch, accelerations (at three locations), wave profile (encountered and stationary), hull bottom pressures, and high-speed video were recorded during each test run. The high-speed video was taken (using a Phantom Miro 320 by Vision Research) looking at the model from the side. Pressure measurements were taken on the bottom of the hull using surface-mounted piezoelectric quartz point sensors (PCB Piezoelectrics, model 113B27 and 113B28). The locations of the pressure sensors at a single longitudinal position are given in Table 1 and shown in Figure 1. The pressure sensors were sampled at a rate of 20 kHz. All other measurements were sampled at a rate of 5 kHz.

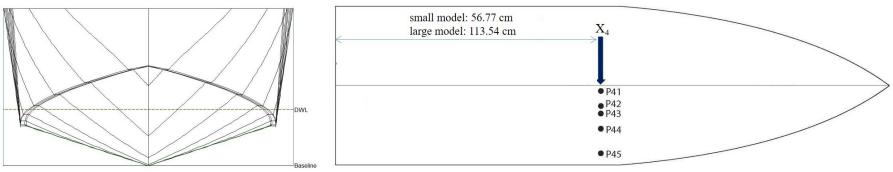

Figure 1. Model body plan and pressure sensor locations

Two model sizes were tested, one a 2.4 m (7.92 ft) and one a 1.4 m (4 ft) length. The geometry was scaled from a full-scale 13.0 m (42.8 ft) prismatic planing craft. The characteristics of the models and full-scale hull are given in Table 1. The smaller model was tested at a single speed, scaled to a corresponding Froude number of 1.84, based on length. The larger model was tested at this same scaled speed as well as a slower speed corresponding to a Froude number of 1.57, based on length. The regular wave conditions corresponded to the most probable waves from a Breschneider spectrum with a significant wave height of 18.8 cm (7.4 in) and a modal period of 2.4 seconds. The resulting regular wave has a wave height of 12.2 cm (4.8 in) with a wave period of 1.6 seconds.

The advantage of regular waves is that the same impact type can be repeated, thus providing information on variations for the same impact conditions. For each test condition, individual wave encounters were separated and treated as an individual slam events. This paper looks at the results of averaging those individual events and considering the resulting standard deviations.

3. Pressure Distribution Reconstruction (PDR) Method

The Rosen pressure distribution reconstruction method [2] uses the pressure signal recorded at pressure sensors along a transverse strip of the model (at a single longitudinal distance from the transom) and transforms these measurements in time to measurements in space over time. In this model, the longitudinal position X_4 is located 113.54 cm (44.70 in) forward from the transom and has a set of five (P_{41}, P_{42}, P_{43}, P_{44}, P_{45}) pressure

Length Overall (L), m (ft)	13.0 (42.8)	2.4 (7.92)	1.2 (4)
Max beam (B), m (ft)	4.0 (13.1)	0.74 (2.4)	0.37 (1.2)
Displacement, metric tons (lbs)	15.9 (35,000)	0.104 (223)	0.013 (27.9)
LCG, m (ft) fwd of transom	4.6 (15.1)	0.85 (2.80)	0.43 (1.41)
Deadrise	18°		
Scale Factor	-	5.4	10.7
Longitudinal pressure sensor locations (x), cm (inches) measured fwd of transom	-	113.54 (44.70)	56.77 (22.35)
x/L position of pressure sensors	-	0.47	
Transverse pressure sensor locations (y) cm (inches) measured from keel	-	2.29 (0.90) 8.69 (3.42) 11.89 (4.68) 18.34 (7.22) 28.85 (11.36)	1.14 (0.45) 4.34 (1.71) 5.94 (2.34) 9.17 (3.61) 14.43 (6.68)
y/B position of pressure sensors	-	0.031 0.119 0.163 0.251 0.394	

Table 1. Hull Characteristics

sensors. The positions of the pressure sensors in this transverse section on the model are given in Table 1 and shown in Figure 1. There is a time history for each impact from each sensor. Figure 2 (left plot) shows the time histories from the sensors during a single impact event. The peak pressure due to the impact moves from the keel to the chine over the time duration of the wave slam and so each sensor records a sudden increase and maximum pressure at a different time, with the time of maximum pressure occurring later in time for sensors further from the keel. The Pressure Distribution Reconstruction (PDR) method attempts to track the pressure pulse front, shown by circles in the left plot of Figure 2, and then each subsequent pressure pulse, where the stars in Figure 2 show a sample single pulse, from sensor to sensor. This provides a relationship between the position of the pressure pulse front and time. By assuming the pressure front maintains a constant velocity between sensors, the pressure measurements following the pressure front can be propagated along the transverse section of hull.

The pressure distribution reconstruction (PDR) allows an approximation of the two-dimensional pressure contour along a longitudinal slice of hull to be calculated for each time step during the hull-wave impact. The assumptions of linear pressure change as a pressure segment moves from one measured location to the next and the assumption of sudden changes in velocity in the pressure pulse as the front reaches each sensor while maintaining constant velocity between measured locations can introduce some error to the pressure distribution. However, due to very large sampling rates for the pressure sensors and relatively closely spaced sensors, the resulting pressure distributions appear reasonable. Figure 2 (right plot) shows the PDR results from a single wave impact event. Rosen [2] found good comparisons when evaluating this method.

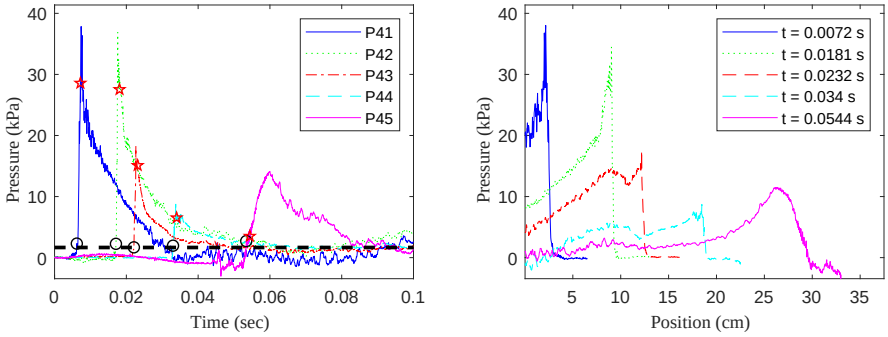

Figure 2. Pressure sensor data for a single impact event. The plot on the left shows the time history from the sensors. The thick dashed line represents the threshold value used to determine the arrival of the pressure wave front, the circles identify the first pressure measurement identified as part of the pressure pulse front, and the stars indicate the passage of an individual pressure pulse part from one sensor to the next. The plot on the right shows the reconstructed pressure distribution for the same impact event. The data is for the large model at 9 m/s (29.5 ft/s).

4. Predicted Bottom Pressures during Wave Slams Method

To provide some comparison for the PDR technique, the transverse pressure distribution is also calculated using an empirically-based, closed-form solution developed by Morabito [3]. That paper presents a set of empirical equations for the pressure distribution on prismatic planing hulls operating in calm water. The method can provide the total pressure on the bottom of the planing hull (both the hydrodynamic and hydrostatic pressure components) at longitudinal locations. Morabito suggests a modification for using the method to predict impact pressures on the bottom of a planing craft slamming in waves by using an adjusted "equivalent planing speed." This equivalent planing speed depends on the relative velocity of the hull and wave surface, an approximation of the spray root location, and the relative trim between the hull and the water surface.

Since the pressure sensors used during testing could only measure the dynamic pressure, only the dynamic pressure values are calculated and presented in this paper. To determine the equivalent planing speed the relative position between the wave and the hull is needed, but this was not recorded during testing. An approximation of the hull-water intersection was based on images from the high-speed video and the timing of the spray root location as determined by the timing of the pressure pulse front passing the pressure sensors. The actual hull orientation along with the vertical and pitching velocities, as measured, are used in the predictions. As with the PDR method, the multiple impact events for the same test condition (in regular waves) were averaged and standard deviations calculated.

5. Results and Discussion

The hull bottom pressures were measured at location X_4 for both model sizes in regular waves. Table 2 shows the variability of the regular wave impact events. The three conditions considered are two speeds for the large model and one speed for the small model. The first row in the table shows the average wave amplitude as well as the standard de-

	Large Model 9.0 m/s (29.5 ft/s)	**Large Model** 7.6 m/s (25 ft/s)	**Small Model** 6.4 m/s (21 m/s)
Regular Wave Amplitude, cm (in)	average = 4.73 (1.86) st. dev≐ 0.118 (0.047) st. dev. = 2.50% of mean amp.	average = 4.96 (1.95) st. dev. = 0.19 (0.074) st. dev. = 3.80% of mean amp.	average = 2.04 (0.80) st. dev. = 0.194 (0.077) st. dev. = 9.52% of mean amp.
Model Heave Amplitude, cm (in)	average = 2.48 (0.98) st. dev≐ 0.173 (0.068) st. dev. = 6.98% of mean amp.	average = 2.46 (0.97) st. dev. = 0.057 (0.022) st. dev. = 2.31% of mean amp.	average = 1.11 (0.44) st. dev. = 0.42 (0.17) st. dev. = 38.2% of mean amp.
Model Pitch Amplitude, degrees	average = 1.66 st. dev≐ 0.093 st. dev. = 5.61% of mean amp.	average = 1.52 st. dev. = 0.06 st. dev. = 3.85% of mean amp.	average = 0.91 st. dev. = 0.29 st. dev. = 31.4% of mean amp.
Vertical Acceleration LCG, m/s^2 (ft/s^2)	maximum = 8.96 (29.4) st. dev≐ 0.35 (1.14) st. dev. = 3.88% of max.	maximum = 10.14 (33.25) st. dev. = 0.31 (1.01) st. dev. = 3.04% of max.	maximum = 10.9 (35.8) st. dev. = 1.82 (5.97) st. dev. = 17.7% of max.
Vertical Acceleration Bow, m/s^2 (ft/s^2)	maximum = 49.0 (160.9) st. dev≐ 1.52 (4.97) st. dev. = 3.09% of max.	maximum = 44.0 (144.3) st. dev. = 1.38 (4.54) st. dev. = 3.14% of max.	maximum = 42.9 (140.6) st. dev. = 4.37 (14.33) st. dev. = 10.2% of max.

Table 2. Regular Wave Measurement Repeatability

viations, as well as presenting the standard deviation as a percentage of the mean amplitude. The large model waves are very repeatable with standard deviations less than 4% of the mean amplitude value. The small model waves show larger levels of variability with the standard deviation close to 10% of the mean amplitude. The smaller wave is more difficult for the wavemaker in the tank to create, so there is more variation in the size of each regular wave.

The other rows in the table show the model heave, pitch, and vertical accelerations, which represent the motions and forces acting on the model during the wave impact event. The large model motions in these regular wave tests are reasonably repeatable, with standard deviations much less than 10% of the motion amplitudes for heave and pitch. The maximum vertical accelerations recorded at the longitudinal center of gravity (LCG) and forward perpendicular (Bow) are also consistent with standard deviations less than 4% of the maximum measured acceleration. The small model motions are much less repeatable with the heave and pitch standard deviations over 30% of the motion amplitudes. The maximum vertical accelerations at the LCG and Bow are more consistent than the model motions, but the standard deviations are still between 10 and 20% of the maximum vertical accelerations. The relative amount of variability for the different tested condition shown in the pressure sensor signals seen in Figure 3 is typical and shows that the small model record has greater variability than for the large model during these wave impact events.

These pressures measured on the bottom of the hull should relate to the forces acting on the model, so if the motions and forces are repeatable, the pressures measured during each impact event should also show strong correlation. As seen with the motions and accelerations, the large model measurements have much less variability than the small model measurements. Figure 3 shows the mean pressure signals with the standard deviations based on the multiple impacts for each test condition for the sensors. The variation for sensors for all testing conditions increases as the sensor position moves away from the keel and towards the chine. In addition, the peak magnitude of the pressure signal generally decreases as the sensor position moves further from the keel. However, the pressure signals show good consistency with respect to the sudden increase of the pressure pulse front and the general trend for the pressure signal over time.

Figure 4 shows the averaged pressure distribution reconstruction (PDR) based on the pressure signals. The dotted lines represent the range of standard deviation for the

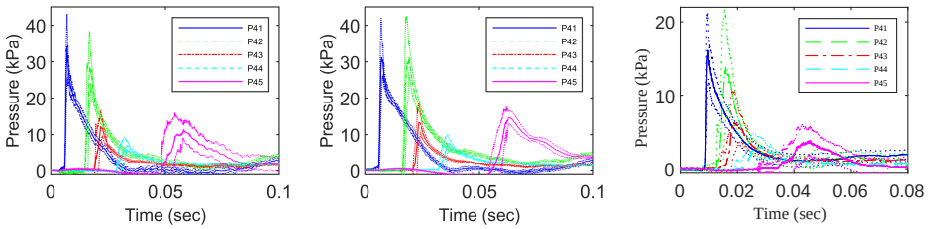

Figure 3. The average pressure signals measured at each pressure sensor with standard deviation (dotted lines) shown for large model - 9 m/s (29.5 ft/s), large model - 7.6 m/s (25 ft/s), and small model - 6.4 m/s (21 ft/s) from left to right, respectively.

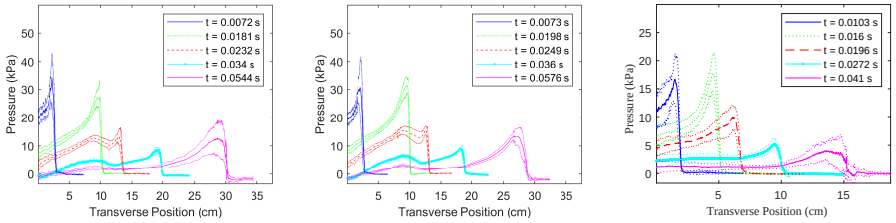

Figure 4. The average pressure distribution reconstruction at different times during a single wave slam event shown for large model - 9 m/s (29.5 ft/s), large model - 7.6 m/s (25 ft/s), and small model - 6.4 m/s (21 ft/s) from left to right, respectively. Each line represents the pressure distribution acting over the X_4 longitudinal position of the hull at different times.

averaged pressure distribution signals. The averaged pressure distributions in Figure 4 look very similar to the single impact pressure distribution reconstruction shown in Figure 2 (right plot). For this test condition the pressure distribution shows a sharp increase and spike near the beginning of the impact while the pressure front is near the keel. As the spray root of the water-hull impact moves from the keel to the chine the pressure peak magnitude generally decreases until the spray root passes the sensor P44. From this location the pressure peak magnitude increases again. In addition to the changes in the pressure peak magnitude, the pressure distribution reconstructions show the pressure spike smoothing out over the duration of the impact event.

One unusual element of this pressure distribution is the double hump aspect seen at $t = 0.0232$ and $t = 0.034$ seconds for the left plot in Figure 4. At the location of P42, the pressure signal did not reduce in magnitude as much as the pressure does closer to the chine but the magnitude increases again at sensor P43. The hull motion measurements show that there is an inflection in the pitch signal during this time frame. The model begins the impact with a bow down pitch motion, but as the impact occurs the bow down pitching motion slows and changes to be a bow up pitching motion. The vertical acceleration at the bow reaches the maximum value during this time frame. The maximum vertical acceleration at the LCG occurs later and the double hump may be related to the effects of the maximum accelerations at the bow while the vertical acceleration at the LCG is still increasing.

Another interesting aspect of the pressure distribution reconstruction is the increase in pressure as the water-hull spray root approaches the chine ($t = 0.034$ to $t = 0.0544$, as seen in the left plot of Figure 4). In this region the pitch is moving in a bow up

direction, but it starts to slow and goes through another inflection point. The acceleration at the LCG has reached the initial peak and has a local minimum. This fluctuation in the acceleration signal may explain the increase in pressure on the hull during this time. This pressure increase is likely due to a temporary increase in impact velocity during the wave slam event, as the increase in pressure is seen in the raw pressure sensor data as shown in Figure 3.

The middle plot in Figure 4 shows the averaged pressure distribution reconstruction for the large model traveling at 7.6 m/s (25 ft/s). The pressure distributions shown are for the times when the pressure pulse front reaches each of the pressure sensors. The shapes are very similar to the faster speed condition shown in the far left plot of Figure 4, including the double hump behavior for the third and fourth times and the increase in pressure peak as the pulse moves out closer to the chine. As would be expected, since the forward speed is slower, this condition shows the pressure pulse front traveling at a slower pace from the keel to the chine. The pulse front reaches the pressure sensors at later times (as seen by comparing the times in the legends between the middle and left plots in Figure 4). Interestingly, however, the pressure magnitudes do not seem smaller for the slower forward speed impact events.

The right plot in Figure 4 shows the averaged pressure distribution reconstruction for the small model traveling at 6.4 m/s (21 ft/s). The pressure distributions are for the times when the pressure pulse front reaches each of the pressure sensors. The general shape of the pressure distributions match those for the large model at the equivalent speed (shown in the left plot of Figure 4). Compared with the two large model slam conditions, the pressure distributions show larger standard deviations, matching the trend in increased variability from the model motions and pressure time history data. The pressure peak magnitudes for the small model are approximately half those for the large model. The small model pressure distribution does not show the double hump for any of the times shown, nor does the pressure peak increase as the pressure pulse front approaches the chine. The small model vertical acceleration measurement does not show the oscillations seen in the large model impact events, therefore there is no local acceleration minimum during the slam event. This difference in pressure distribution supports the claim that the increase in pressure peak as the pulse approaches the chine is due to the local minimum in the vertical acceleration record - the small model shows no local minimum and the pressure peak continues to decrease as it approaches the chine. For the double hump, the small model maximum vertical acceleration at the bow occurs much closer to the maximum vertical acceleration at the LCG (accounting for the time scaling). The double hump in the transverse pressure distribution may be related to the larger pitching motion of the large hull and the longer time delay between the maximum vertical acceleration at the bow and the LCG.

Figure 5 shows the comparison of the averaged reconstructed pressure distributions with the averaged predicted pressure distributions (left plot) as well as the standard deviations based on the repeated impact events (right plot). Overall, the pressure predictions based on the measured hull information and empirical equations is fairly repeatable with reasonable ranges shown for the standard deviations over the course on the impact event (right plot in Figure 5). The timing of the pressure progression from keel to chine agrees closely between the predicted and reconstructed pressure distributions (shown in left plot of Figure 5). The predicted pressure distribution also captures the increase in pressure peak magnitude as the pressure pulse front nears the chine. This supports the claim that

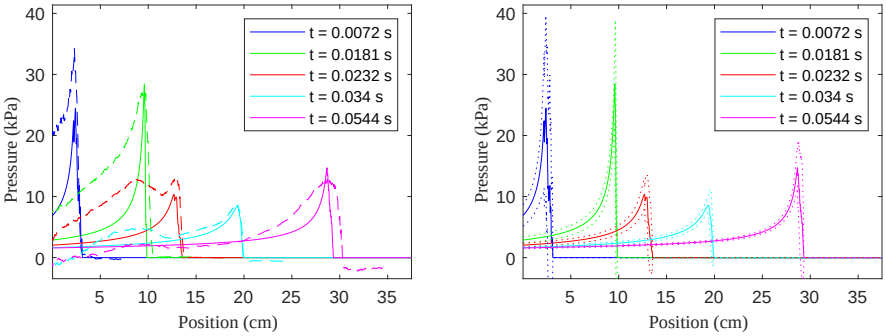

Figure 5. Comparison of the predicted and reconstructed pressure distributions for a single impact for the large model at 9 m/s (29.5 ft/s). In the left plot, the solid lines show the predicted pressure distributions at five times during the impact and the dashed lines show the reconstructed pressure distributions at those times. The right plot shows the predicted pressures with the standard deviations (indicated by the dotted lines).

the increase in pressure magnitude is related to the motions of the hull during this interval. The predicted pressure distributions have a consistent shape as the pressure pulse front moves from the keel to the chine. The shape has general agreement with the reconstructed pressure distribution (a somewhat gradual increase to a maximum followed by a sharp drop in pressure), but the reconstructed pressure distributions are not a consistent shape as the impact progresses. For instance, the predicted pressure distributions fail to capture the double hump behavior seen in the reconstructed pressures. This difference suggests that the double hump is not caused by hull motions, but related to dynamic changes from the impact (the predictions are based on a quasi-static analysis at each instant) or a artifact of the PDR method. Since the small model reconstructed pressures do not show this double hump behavior, it is more likely the distribution based on the measured pressures varies due to dynamic effects not included in the prediction method.

The different total integrated pressures over a transverse section of the hull between the reconstructed and predicted models, indicate the force calculated from the models would be significantly different. Based on the results shown in Figure 5 (left plot), using the predicted pressures would result in an under-prediction of the slamming force. Modificiations to the empirical relationships used in the predictive model for slamming pressures (as opposed to the current calm water relationships) could improve the predictions for force.

6. Conclusions

The PDR method described by Rosen [2] allows the spatial pressures on the bottom of the hull to be determined during a wave slam. The Morabito pressure distribution method [3] allows these spatial pressure distributions to be predicted using calm water empirical equations with an adjusted equivalent forward speed to account for instantaneous hull position and velocity relative to the water surface. Using measured pressures from a planing hull tested in regular waves and both methods described allowed estimates of variability for spatial pressures on the hull bottom during hull-wave slamming. Combining these features can provide insights into the physics of how the hull and water interact during slamming events.

References

[1] Allen, R.G. and Jones R.R. A simplified method for determining structural design-limit pressures on high performance marine vehicles. Proceedings of the AIAA/SNAME Advanced Marine Vehicles Conference; 1978; San Diego, CA (USA).

[2] Rosen, A. Impact pressure distribution reconstruction from discrete point measurements. International Shipbuilding Progress 2005; 52 (1): 91-107.

[3] Morabito, M. Empirical Equations for planing hull bottom pressures. Journal of Ship Research 2014; 58 (4): 185-200.